Coupling cyclostationarity and Near-field Acoustic Holography for bearing fault recognition

Corentin Chesnais[1], Jean-Hugh Thomas[1,2] and Jean-Claude Pascal[1,2]

[1]Laboratoire d'Acoustique de l'Université du Maine (LAUM UMR-CNRS 6613)
rue Olivier Messiaen 72085 Le Mans Cedex 09, France
[2]Ecole Nationale Supérieure d'Ingénieurs du Mans (ENSIM)
rue Aristote 72085 Le Mans Cedex 09, France
corentin.chesnais@gmail.com, {jean-hugh.thomas, jean-claude.pascal}@univ-lemans.fr

Abstract

The goal of the study is to demonstrate the interest of taking into account the cyclostationary properties in rotating machinery for monitoring rolling element bearings. The problem consists in recognizing four different bearing states from signals recorded on the machine : the safe state and identified defects on the inner race, on the outer race and on the rolling elements. Two approaches are presented. The first one is based on pattern recognition. Some patterns are composed of features extracted from Power Spectral Densities of acoustic and vibration signals. Other patterns are built using Spectral Correlation Densities of vibration signals. A projection of the patterns using a Principal Component Analysis underlines the effectiveness of the parameters highlighting the cyclostationary property of the data, to separate the different classes of bearing states. The second approach is based on an adaptation of Near-field Acoustic Holography (NAH) to take into account cyclostationarity. NAH is an imaging technique based on the acquisition of the sound field in the Near-field of the sources from a microphone array. It provides a reconstruction of the sound field on the source plane presented as images which allow one to localize and characterize the radiated noise. Since the phenomena taking place within a machine cycle in rotating machinery produce rhythmic events, the acoustic signals acquired highlight cyclostationary properties. It is then relevant to adapt the measurement methods by using these properties. The cyclostationary Near-field Acoustic Holography (CYNAH) was proposed by Wan and Jiang for this purpose [1]. The method is described in the paper and compared to standard NAH. An experiment is also presented using a microphone array moved by a two-axis robot in the near-field of the machine. Some preliminary images to characterize the sound field generated by the machine, equipped with different bearings, are given.

1 Introduction

The study presented here is a preliminary work aiming at establishing the diagnosis of bearings on a rotating machine using acoustic imaging techniques. The idea is to extract some features from the images to feed a diagnosis process to recognize the different defects of the bearings. Few works in the literature deal with this approach [2, 3]. However, many signal processing techniques were investigated on the subject. Some examples are, modeling the time vibration signals with an autoregressive process

to feed a neural network for the decision [4], filtering the signal using wavelets to extract the relevant frequencies [5], applying the spectral kurtosis [6] or composing a pattern with various parameters such as the kurtosis, the root mean square value, the energy, extracted from the acquired signal to feed a neural network optimized by a genetic algorithm [7]. The pattern recognition approach used in the last reference is attractive as any signal processing tool can be used to extract relevant features [8]. When the signals under study present the cyclostationarity property, some papers demonstrate the interest in extracting information using the cyclic power spectrum or the spectral correlation density [9, 10, 11] and especially in the case of bearings diagnostics [12, 13, 14]. The rotating machine involved is the Machinery Fault Simulator of Technivib company. Three faulted bearings and a safe one are used. The defects concern the inner race, the outer race and the rolling elements.

The first work, presented in section 2, consists in underlining the advantage of exploiting the cyclostationarity of the signals using a pattern recognition approach based on a multidimensional analysis. Two pattern vectors are proposed for this goal, one based on features extracted from Power Spectral Densities, the other one from parameters extracted from Spectral Correlation Densities. Some theory on the Cyclic Power Spectrum and the Spectral Correlation Density is also given. Results from experiments are presented. The second work, described in section 3 consists in coupling cyclostationarity and an imaging technique (Near-field Acoustic Holography) to extract information to separate the different classes of bearings. The method called CYNAH is described and compared with standard NAH. Finally a very preliminary result is given.

2 Multidimensional analysis

2.1 Methodology

The aim of the first step is to extract relevant information able to characterize the different states of the bearings. This step requires the use of signal processing tools suitable for the analysis in the sense that they succeed in highlighting parameters whose values are different according to the bearings considered. In the study the Power Spectral Density and the Spectral Correlation Density are used. Then each signal acquired is associated with a pattern vector composed of the parameters extracted from these tools.

It is interesting to see whether the total amount of patterns could be classified with regard to the defect of the bearings. The pattern recognition approach consists in projecting the data into a multidimensional space where each pattern is represented by a point. Thus two similar patterns are close to each other in the representation space. For a pattern composed of several features (more than three), it is not possible to see the cloud of patterns. However, a Principal Component Analysis can provide the view [15]. Indeed, the aim of this analysis is to find a space of smaller dimension to project the data by minimizing the loss of information. The goal here is to provide a data view into a plane, representative of the original data. At this stage, the purpose is not to give a discrimination rule to classify automatically the patterns but to establish the relevance of the parameter extraction step. If the patterns associated with the same bearings are clustered together, the features are supposed to be relevant. The feature extraction is first done using parameters provided by the Power Spectral Density. Then the pattern vector is composed of parameters given by the Spectral Correlation Density to take advantage of the cyclostationarity property of the data.

2.2 Set-up

Two data sets of 20 measurements are made for each bearing using an accelerometer PCB 333M07 of sensitivity 10.2 mV/(ms^{-2}) in the frequency band [0.5-3000 Hz], mounted on the bearing housing, sensitive to the vertical vibrations. The engine speed is controlled at 3000 RPM. Acoustic signals are also recorded by a PCB 130D21 microphone in the frequency band [0.5-9000 Hz], positioned 31cm from the bearing. Two sampling frequencies are used: 25600 Hz and 5120 Hz. 16384 samples are recorded. The first data set is used to compose the pattern vectors based on the computation of the Power Spectral Densities of the signals. The second data set, acquired with the lower frequency rate, is devoted to feature extraction from the Spectral Correlation Densities.

2.3 Pattern vectors based on a frequency analysis

Several pattern vectors are tested using vibration data and then acoustic signals. The PSD of the signals are estimated using Welch periodograms on 1024 spectral lines with 50 % of overlapping leading to a frequency resolution Δf=25 Hz. The first pattern is composed of the DSP taken on 121 frequencies in the [0 3000 Hz] band of the vibration signals. The second pattern has 201 components characterizing the frequency content of the acoustic signals in the [0 5000 Hz]. Two patterns of smaller dimension are also built. They come from a previous study made with the same machine at the same engine speed [3]. From a theoretical point of view, in the presence of defects, typical frequency peaks are expected to appear in the power spectra of the vibration signals [16]. These peaks depend on coefficients usually given by the bearing manufacturers. Thus, the third pattern is composed of the amplitudes of 7 peaks resulted from the examination, done in [3], of the matching between the experimental PSD and the theoretical frequencies. In that study, it was shown that only taking into account the theoretical peaks do not lead to the best results in terms of defect discrimination. To enhance the classification, another pattern was proposed, with 6 components carefully selected from the observation of the experimental DSP of the signals provided by each bearing. That pattern vector is also tested on the data described in section 2.2.

Each DSP or each time signal is associated with a pattern. The aim of PCA is then to project the 80 patterns in a plane in order to highlight their similarities. Figure 1 shows the projections obtained with the different pattern vectors. Note that the axis of the graphs are different for each pattern vector.

Three projections (a, c, d) almost separate the four different classes of defects. When the patterns are composed of a few theoretical peaks, there is an ambiguity to discriminate between the safe bearing and that with defects in the outer or in the inner race. It was the same conclusion in [3]. It appears that the whole frequency content recorded by an accelerometer or a microphone is relevant to separate the classes (a,c). The disadvantages of the pattern vectors involved in (a,c) come from the number of components. The frequency content of the vibration signal does not seem very effective to separate the defects from the outer race and the inner race whereas the frequency content of the acoustic signal succeeds in this separation. On the contrary, some acoustic patterns belonging to the safe class seem close to that corresponding to the bearing with defects in the outer race [see figure 1 (b)]. At last, the use of few components in the pattern vector enables to cluster patterns [see figure 1 (d)] from the same class even if the result is not as demonstrative as in [3]. It is possible that such a selection is required periodically during the life of the bearing. Note that the features in the last case belong to [0 1000 Hz] frequency interval.

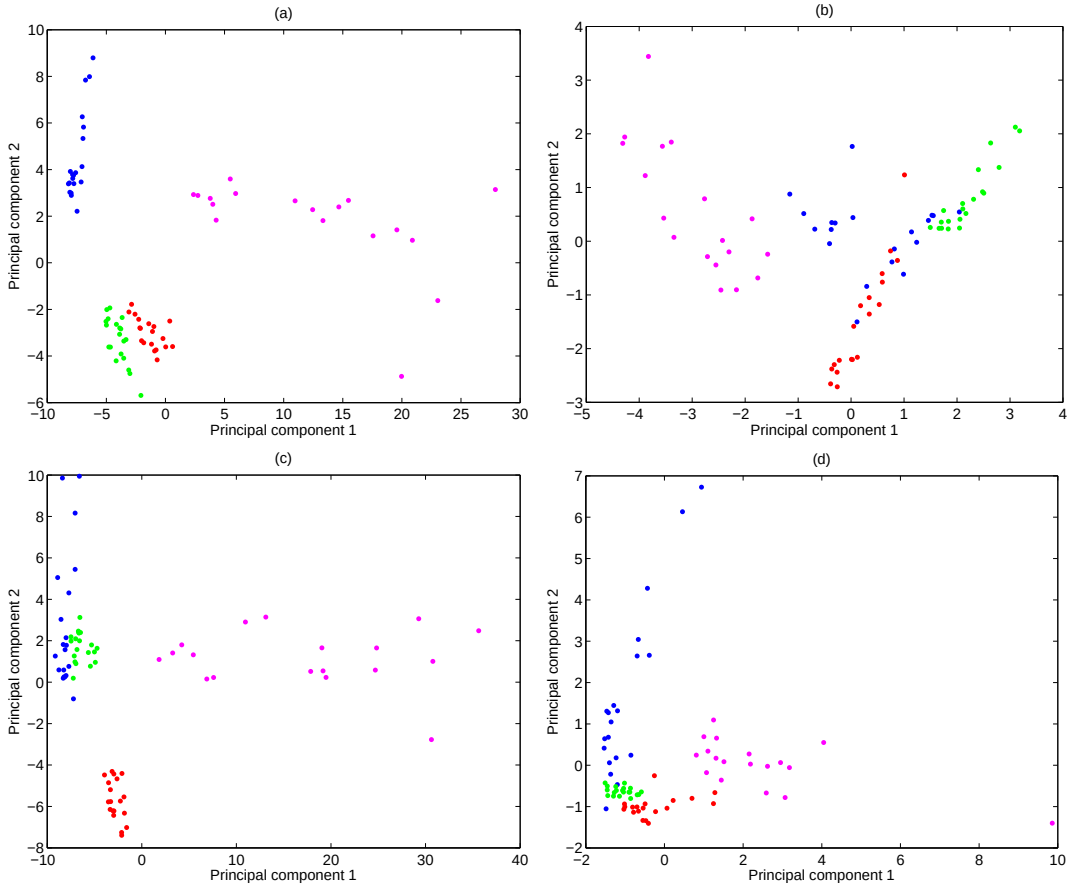

Figure 1: Principal Component Analysis of the 80 patterns (a) in dimension 121 for vibration signals, (b) in dimension 7 for vibration signals, (c) in dimension 361 for acoustic signals, (d) in dimension 6 for vibration signal. 71 %, 88 %, 71 % and 76 % of the initial information are respectively kept. The colours of the points depend on the bearing considered (safe bearing in blue, bearing with defects in the outer race in red, in the inner race in green, in the ball spin in magenta).

2.4 Pattern vector based on cyclostationarity features

Only one pattern vector is tested, built from the vibration signals. 19 feature are chosen which are extracted from the spectral correlation densities defined theoretically in the next section.

2.4.1 Cyclic Power Spectrum and Spectral correlation

The instantaneous autocorrelation of a signal $x(t)$ is defined as

$$R_x(t,\tau) = E[x(t+\tau/2)x^*(t-\tau/2)], \tag{1}$$

where $E[.]$ denotes the mean value, τ the time-lag and t is linked to the starting time. For a cyclostationnary signal, the instantaneous correlation is periodic with regard to variable t :

$$R_x(t,\tau) = R_x(t+kT_0,\tau), \tag{2}$$

where k is a positive or negative integer. The instantaneous autocorrelation, periodic with period T_0, can be decomposed into Fourier series as

$$R_x(t,\tau) = \sum_{n=-\infty}^{+\infty} c_n(\tau)e^{2j\pi nt/T_0}, \tag{3}$$

where $c_n(\tau)$ are the Fourier coefficients. Consider α the cyclic frequency $1/T_0$ and $\alpha_n = n\alpha$ its harmonics, Eq. (3) is rewritten

$$R_x(t,\tau) = \sum_{n=-\infty}^{+\infty} c_n(\tau)e^{2j\pi\alpha_n t}, \tag{4}$$

$$R_x(t,\tau) = \sum_{\alpha_n} R_x^{\alpha_n}(\tau)e^{2j\pi\alpha_n t}, \tag{5}$$

that exists usually in the literature as

$$R_x(t,\tau) = \sum_{\alpha} R_x^{\alpha}(\tau)e^{2j\pi\alpha t}, \tag{6}$$

where $R_x^\alpha(\tau)$ is the cyclic autocorrelation function. The cyclic power spectrum$S_x^\alpha(f)$ is the Fourier transform of the cyclic autocorrelation function :

$$S_x^\alpha(f) = \int_{-\infty}^{+\infty} R_x^\alpha(\tau)e^{-j2\pi f\tau}d\tau. \tag{7}$$

The cyclic power spectrum depends on two variables, the spectral frequency f and the cyclic frequency α. The resolution on the cyclic frequency axis is $\Delta\alpha = \alpha$ and that on the spectral frequency Δf depends on the size of the cyclic autocorrelation function. The spectral correlation function is defined as

$$S_x(\alpha,f) = \lim_{T\to\infty} E[X_T(f+\alpha/2)X_T^*(f-\alpha/2)], \tag{8}$$

where $X_T(f)$ is the Fourier transform of $x(t)$ on the time interval T. It is effective to implement the spectral correlation by the use of the averaged cyclic periodogram [14]. The resolution on the cyclic frequency of $S_x(\alpha,f)$ is finer than that of the cyclic power spectrum. Indeed it is just limited by the length of the record. The resolution on the spectral frequency depends on the size of the averaged segments.

2.4.2 Results

The spectral correlation densities (SCD) are computed for the signal of the second data set. Some examples of the SCD obtained for vibration signals corresponding to the safe bearing and that with defects in the outer race, in the inner race and in the rolling elements are shown in figure 2.

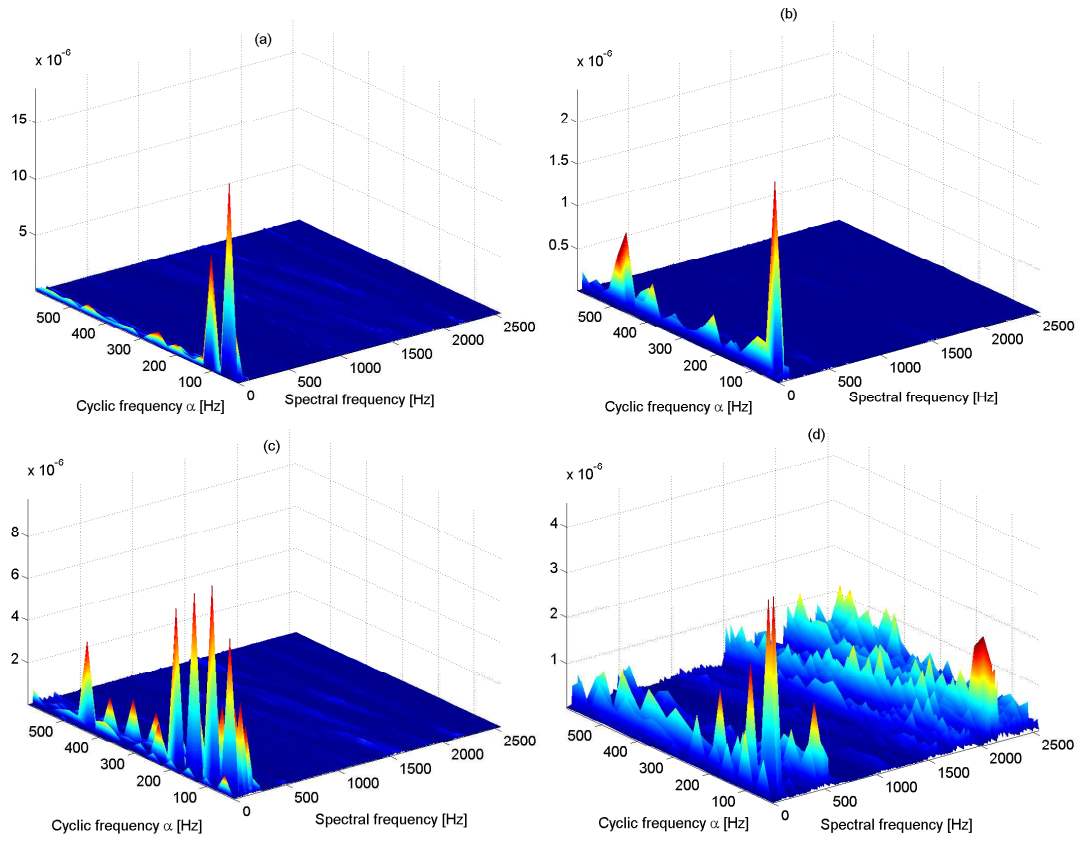

Figure 2: Spectral correlation densities of vibration signal corresponding to (a) the faulty bearing in the outer race, (b) the safe bearing, (c) the faulty bearing in the inner race and (d) the faulty bearing in the ball spin. The resolution in spectral frequencies is $\Delta f = 5$ Hz and the resolution in cyclic frequencies is $\Delta\alpha = 25$ Hz.

The 19 features, chosen to build the pattern vector, are spectral correlation densities for some specific points in the representation given by the couple (f, α) where f is the spectral frequency and α the cyclic frequency. The selected features are shown in figure 3. The cloud of 80 patterns is then projected into a new representation space given by the PCA (see figure 4). The patterns are clustered in their class. The patterns relative to the bearing with defects in the inner race are isolated. The spectral correlation density seems powerful to characterize the vibration signals acquired in the case of faulty bearings.

3 Nearfield Acoustic Holography

3.1 Theory

Nearfield Acoustic Holography (NAH) is an imaging technique providing the acoustic field radiated by a system which generates some noise [17]. Standard holography deals with stationary sources. Here the geometry considered for the reconstruction is planar. NAH is based on the acquisition of the sound

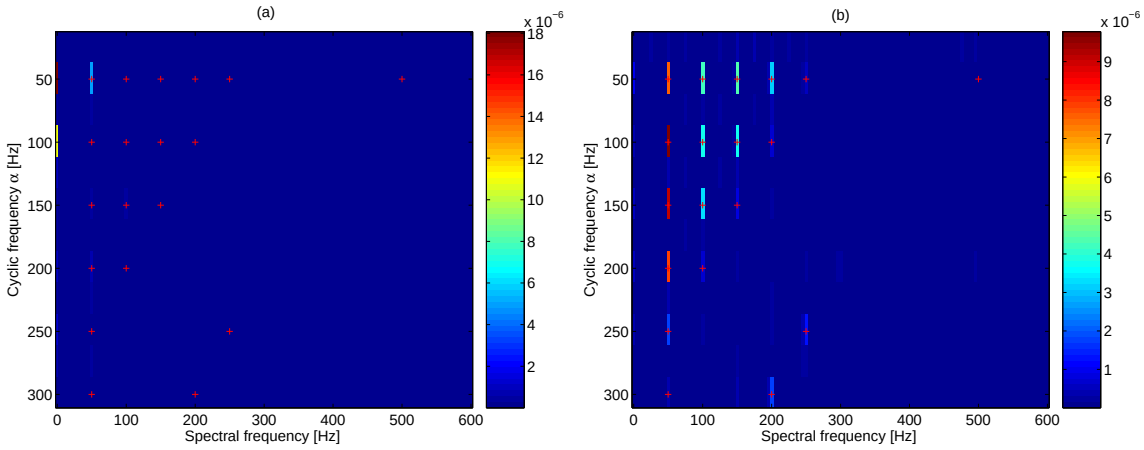

Figure 3: Features extracted from the Spectral correlation densities : red plus signs on the images for signals corresponding to faulty bearings (a) in the outer race, (b) in the inner race.

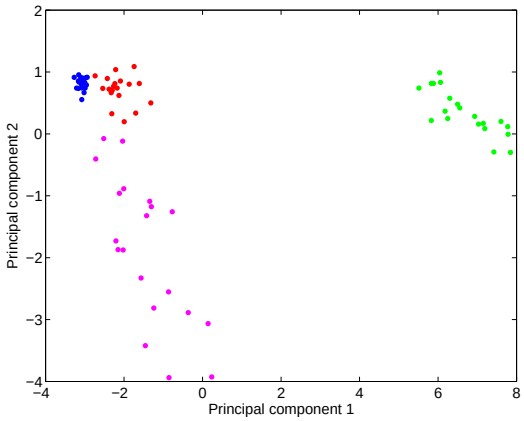

Figure 4: Principal Component Analysis of the 80 patterns built in dimension 19 using the specific combinations (f, α) shown in figure 3. The colours of the patterns depend on the bearing considered (safe bearing in blue, bearing with defects in the outer race in red, in the inner race in green, in the ball spin in magenta).

field in the near-field of the sources of interest using a microphone array. The goal is to solve an inverse problem which consists in backpropagating the acoustic pressure field acquired from the measurement plane to the source plane. This is done for a single frequency or a frequency band which is an input of the algorithm. Processing for reconstruction takes place in the wavenumber domain and thus requires the use of the 2D spatial Fourier transform: the sound field is decomposed into several planar waves with different directions of arrival on the array.

Let us consider $p(x, y, z_H, f_0)$ as the spatial pressure field acquired from the measurement plane $z = z_H$, for the frequency f_0, using a microphone array. The spatial pressure field to recover on the source plane is $p(x, y, z_S, f_0)$. The wavenumber spectrum on the source plane $P(k_x, k_y, z_S, f_0)$ can be deduced from $P(k_x, k_y, z_H, f_0)$ according to

$$P(k_x, k_y, z_S, f_0) = G^{-1}(k_r, \Delta z, k_0)\ \mathcal{R}\ P(k_x, k_y, z_H, f_0), \tag{9}$$

with

$$k_r = \sqrt{k_x^2 + k_y^2}, \quad \Delta z = z_H - z_S, \tag{10}$$

$$G^{-1}(k_r, \Delta z, k_0) = \begin{cases} e^{j\Delta z\sqrt{k_0^2 - k_r^2}} & \text{for } k_r \leq k_0, \\ e^{\Delta z\sqrt{k_r^2 - k_0^2}} & \text{for } k_r > k_0. \end{cases} \tag{11}$$

Δz is the backpropagation distance, G^{-1} the inverse propagator and R is an operator in charge of filtering and regularizing the inverse problem in the wavenumber domain. $k_0 = 2\pi f_0/c$, where c denotes the sound speed, takes an important part of the process in the wavenumber domain. Indeed, the circle of radius k_0 separates two kinds of waves: the propagating waves with wavenumbers inside the circle and the evanescent waves with wavenumbers outside the circle. According to Eq. (11) during the reconstruction, the propagating waves are phase-shifted and the evanescent waves are exponentially amplified. This amplification causes the inversion process in NAH critical. That is why it is necessary to filter [18] the acquired wavenumber spectrum $P(k_x, k_y, z_H, f_0)$ or to use regularization [19] before applying the inverse propagator. The end of the process is based on the inverse 2D Fourier transform of the wavenumber spectrum $P(k_x, k_y, z_S, f_0)$ yielding the sound field on the source plane $p(x, y, z_S, f_0)$.

4 Cyclostationary nearfield acoustic holography

In standard NAH, the pressure field on the source plane is used to be reconstructed for one frequency. Indeed the starting point of the operation is a spatial image of the sound field for one frequency, provided by the application of the Fourier transform operator to each time signal acquired by the microphones. In this case, the cyclostationary property of the signals is not taken into account. The idea of CYNAH is to use the information highlighted by the cyclic power spectrum or the spectral correlation density in the inverse problem solved by NAH. The aim is to obtain $S_p^\alpha(x, y, z_S, f)$ the spatial image of the sound field on the source plane for a couple of parameters involving a spectral frequency f and a cyclic frequency α. Wan et al. claim in [1] that it is not possible to reconstruct $S_p^\alpha(x, y, z_S, f)$ from the sound field on the hologram $S_p^\alpha(x, y, z_H, f)$ because of a loss of phase information. They propose to directly reconstruct the sound field on the source plane from other backpropagated quantities according to the filter property of the cyclic power spectrum [9].

4.1 Filter property of cyclic power spectrum

Consider a reference microphone located closer to the source plane than the array. It can be assumed that $p(t)$ the signal acquired by one microphone of the array results from a linear filtering of the signal recorded by the reference $r(t)$. The convolution product describing the filtering is

$$p(t) = \int_{-\infty}^{+\infty} g(\tau) r(t-\tau) d\tau, \tag{12}$$

where $g(t)$ is the impulse response of the filter. When the signal under study is cyclostationary, the cyclic power spectrum of $p(t)$ is linked to that of $r(t)$ according to

$$S_p^\alpha(f) = G(f+\alpha/2)\, S_r^\alpha(f)\, G^*(f-\alpha/2). \tag{13}$$

A similar equation exhibits the relationships between the spectral correlations of $p(t)$ and $r(t)$:

$$S_p(\alpha, f) = G(f+\alpha/2)\, S_r(\alpha, f)\, G^*(f-\alpha/2). \tag{14}$$

By using the cross spectral correlation $S_{pr}(\alpha, f)$ defined by

$$S_{pr}(\alpha, f) = < P(f+\alpha/2) R^*(f-\alpha/2) >_t, \tag{15}$$

with the time-average operator $< . >_t$, where $P(f+\alpha/2)$ and $R(f-\alpha/2)$ are the spectral components of $p(t)$ and $r(t)$ at frequencies $f+\alpha/2$ and $f-\alpha/2$ respectively, the time-delay property of the spectral correlation leads to the two following equations:

$$S_{pr}(\alpha, f) = G(f+\alpha/2) S_p(\alpha, f), \tag{16}$$

$$S_{rp}(\alpha, f) = S_r(\alpha, f) G^*(f-\alpha/2), \tag{17}$$

where $G(f+\alpha/2)$ and $G(f-\alpha/2)$ are the spectral components of $g(t)$ at frequencies $f+\alpha/2$ and $f-\alpha/2$. The combination of eqs 14, 16 and 17 yields

$$S_p(\alpha, f) = \frac{S_{pr}(\alpha, f) S_{rp}(\alpha, f)}{S_r(\alpha, f)}. \tag{18}$$

4.2 Processing

The technique of CYNAH provides the spectral correlation $S_p(x, y, z_S, \alpha, f)$ on the source plane from the quantities $S_{pr}(x, y, z_S, \alpha, f)$, $S_{rp}(x, y, z_S, \alpha, f)$ and $S_r(\alpha, f)$ using Eq. 18. These quantities are backpropagated from those computed on the measurement plane $S_{pr}(x, y, z_H, \alpha, f)$ and $S_{rp}(x, y, z_H, \alpha, f)$,using G_{pr}^{-1} and G_{rp}^{-1} in the wavenumber domain, in accordance to Eq. 19 and 22.

$$S_{pr}(x, y, z_S, \alpha, f) = \mathcal{F}_{xy}^{-1}\, G_{pr}^{-1}(k_r, \Delta z)\, \mathcal{R}\, \tilde{S}_{pr}(k_x, k_y, z_H, \alpha, f), \tag{19}$$

$$\tilde{S}_{pr}(k_x, k_y, z_H, \alpha, f) = \mathcal{F}_{xy}\, S_{pr}(x, y, z_H, \alpha, f), \tag{20}$$

$$G_{pr}^{-1}(k_r, \Delta z) = \begin{cases} e^{j\Delta z \sqrt{k_{pr}^2 - k_r^2}} & \text{for } k_r^2 \leq k_{pr}^2, \\ e^{\Delta z \sqrt{k_r^2 - k_{pr}^2}} & \text{for } k_r^2 > k_{pr}^2, \end{cases} \tag{21}$$

$$S_{rp}(x, y, z_S, \alpha, f) = \mathcal{F}_{xy}^{-1}\, G_{rp}^{-1}(k_r, \Delta z)\, \mathcal{R}\, \tilde{S}_{rp}(k_x, k_y, z_H, \alpha, f), \tag{22}$$

$$\tilde{S}_{rp}(k_x, k_y, z_H, \alpha, f) = \mathcal{F}_{xy}\, S_{rp}(x, y, z_H, \alpha, f), \tag{23}$$

$$G_{rp}^{-1}(k_r, \Delta z) = \begin{cases} e^{j\Delta z\sqrt{k_{rp}^2 - k_r^2}} & \text{for } k_r^2 \leq k_{rp}^2, \\ e^{\Delta z\sqrt{k_r^2 - k_{rp}^2}} & \text{for } k_r^2 > k_{rp}^2, \end{cases} \tag{24}$$

with $k_{rp} = 2\pi(f - \alpha/2)/c$ and $k_{pr} = 2\pi(f + \alpha/2)/c$. $\mathcal{F}_{xy}$ and $\mathcal{F}_{xy}^{-1}$ are respectively the operators representing the two dimensional spatial direct and inverse Fourier transforms, defined as

$$\mathcal{F}_{xy} \equiv \int_{-\infty}^{+\infty} e^{jk_x} e^{jk_y} dxdy, \tag{25}$$

$$\mathcal{F}_{xy}^{-1} \equiv \left(\frac{1}{2\pi}\right)^2 \int_{-\infty}^{+\infty} e^{-jk_x} e^{-jk_y} dk_x dk_y. \tag{26}$$

The processing to implement CYNAH method is then similar to that used for standard NAH. The same R operator is required in the wavenumber domain. The backpropagators are similar. The differences are linked to the acoustic wavenumber k_0 in standard NAH replaced with wavenumbers k_{rp} and k_{pr} in CYNAH. Backpropagation is required to be implemented twice and it is important to understand that the spatial image resulting from CYNAH processing highlights the spectral correlation of the sound field on the source plane between frequency $f - \alpha/2$ and $f + \alpha/2$.

4.3 Set-up

Acoustic measurements were done for each bearing from a 4 by 4 microphone array which was moved by a two-axis robot at 15 positions, providing an overall scan dimension of 1.2 by 0.72 m^2. Two fixed-location reference microphones are used to recover the phase relationships between the pressure measurements done at different times. The step size between two microphones in both x and y directions is a =0.06 m. The configuration of the experiment provides a frequency band for the analysis of [287 2867]Hz where the minimum and maximum frequencies are given by $f_{min} = c/L$ and $f_{max} = c/2a$ with $L = 1.2$ m. Each hologram was acquired from a measurement plane located 0.2 m from the source plane (passing by the bearing housing) and was backpropagated to the source plane using CYNAH.

4.4 Preliminary results

Preliminary results, which need to be validated, are presented in figure 5. The spatial spectral correlation density is reconstructed on the source plane for the safe bearing and the one with a defect in the inner race for spectral frequencies 300 Hz and 1515 Hz with a cyclic frequency α=50 Hz. The cyclic frequency was obtained experimentally by computing the Fourier transform of the instantaneous autocorrelation function $R_x(t, \tau)$ with respect to variable t and by selecting the first peak. One of the problem here is to choose the most relevant spectral frequency for the recognition task.

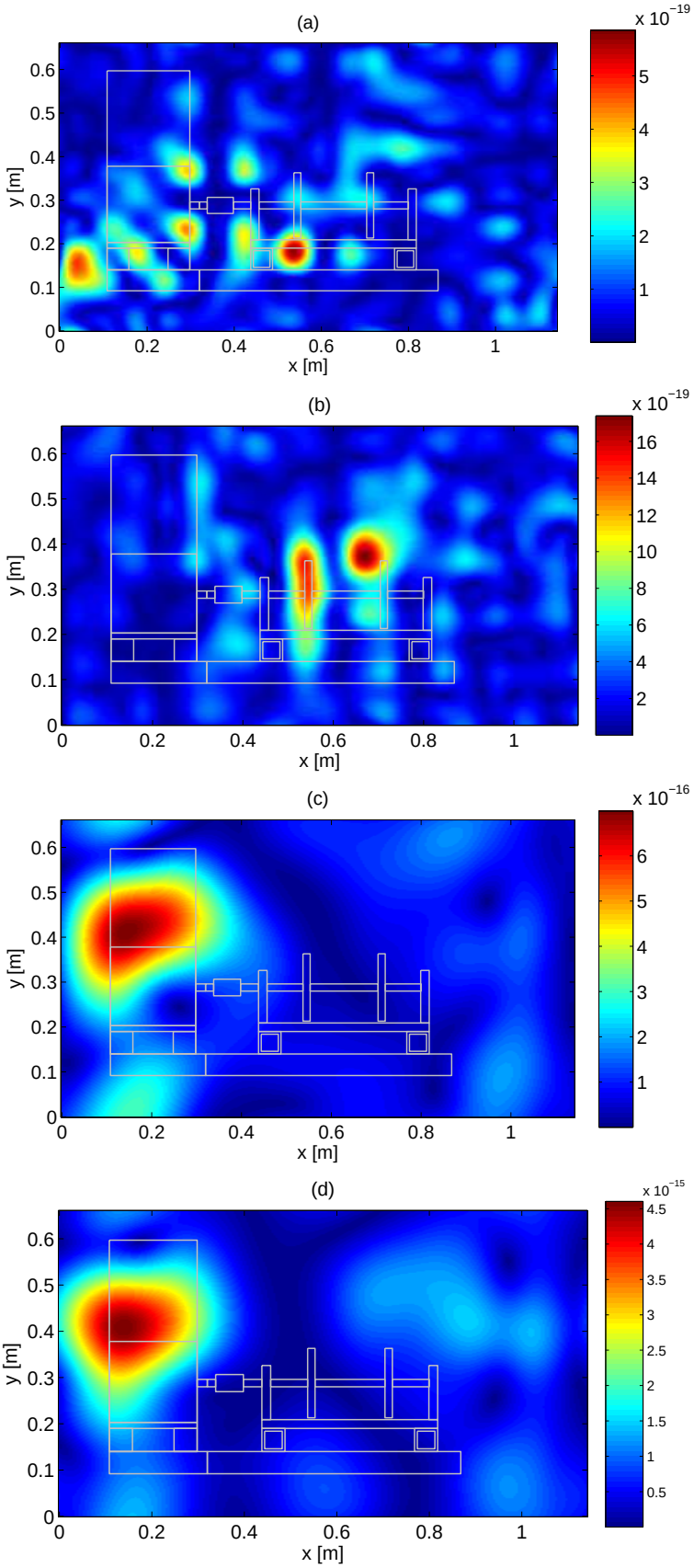

Figure 5: Spatial Spectral Correlation Densities: (a) safe bearing, f=1515 Hz, α=50 Hz, (b) Faulted bearing in the inner race, f=1515 Hz, α=50 Hz, (c) safe bearing, f=300 Hz, α=50 Hz, (d) Faulted bearing in the inner race, f=300 Hz, α=50 Hz.

5 Conclusion

The aim of our study is to recognize four classes of bearings from information extracted on the rotating machine: safe, faulty with defects in the outer race, the inner race and the ball spin. A first work based on pattern recognition showed that the Spectral Correlation Density is very suitable to characterize the bearings. For this purpose a multidimensional analysis was performed on vibration signals to compose patterns, followed by a projection of the cloud of patterns into a discriminated plane using Principal Component Analysis. The use of the same approach with features built from the Power Spectral Densities of acoustic signals also showed the ability of microphones to differentiate the states of the bearings. The cyclostationarity property of the signals was exploited in a second work based on Cyclostationary Near-field Acoustic Holography. The method was carefully studied, implemented and applied to a real case. Preliminary results were given, which require additional developments.

References

[1] Q. Wan, W. K. Jiang, *Near field acoustic holography (NAH) theory for cyclostationary sound field and its application*, Journal of Sound and Vibration 290 (2006) pp. 956-967.

[2] W. Lu, W. Jiang, H. Wu, J. Hou *A fault diagnosis scheme of rolling element bearing based on near-field acoustic holography and gray level co-occurrence matrix*, Journal of Sound and Vibration 331 (2012) pp. 3663-3674.

[3] P. Coutable, J.-H. Thomas, J.-C. Pascal, and F. Eveilleau, *Bearing fault detection based on Near-field Acoustic Holography*, *Proceedings of Surveillance6 Conference*, Compiègne (October 2011).

[4] D. C. Baillie and J. Mathew, *Fault diagnosis of bearings using short data lengths*, *Condition Monitoring and Diagnostic Engineering Management (COMADEM)*, New Delhi (1994).

[5] J. Liu, W. Wang, F. Golnaraghi, and K. Liu, *Wavelet spectrum analysis for bearing fault diagnostics*, Measurement Science and Technology (2008) pp. 1-9.

[6] V. Vrabie, P. Granjon, C.-S. Maroni, and B. Leprettre, *Application of spectral kurtosis to bearing fault detection in induction motors*, *Proceedings of Surveillance5 Conference*, Senlis (October 2004).

[7] L. Padovese and S. Vicente, *Optimizing probabilistic neural networks by the use of genetic algorithms for rolling bearing fault diagnosis*, *Proceedings of Surveillance5 Conference*, Senlis (October 2004).

[8] S. Theodoridis and K.Koutroumbas, *Pattern recognition*, Academic Press, San Diego (1999).

[9] W. Gardner, *Exploitation of spectral redundancy in cyclostationary signals*, IEEE Signal Processing Magazine (1991) pp. 14-36.

[10] J. Antoni, *Cyclic spectral analysis in practice*, Mechanical Systems and Signal Processing 21 (2007) pp. 597-630.

[11] J. Antoni, *Cyclostationarity by examples*, Mechanical Systems and Signal Processing 23 (2009) pp. 987-1036.

[12] R. B. Randall, J. Antoni, *Rolling element bearing diagnostics- A tutorial*, Mechanical Systems and Signal Processing 25 (2011) pp. 485-520.

[13] J. Antoni, R. B. Randall, *On the use of the cyclic power spectrum in rolling element bearings diagnostics*, Journal of Sound and Vibration 281 (2005) pp. 463-468.

[14] J. Antoni, *Cyclic spectral analysis of rolling-element bearing signals: Facts and fictions*, Journal of Sound and Vibration 304 (2007) pp. 497-529.

[15] G. Saporta, *Probabilités analyse des données et statistique*, Technip, Paris (1990).

[16] R. Bigret, J.-L. Féron *Diagnostic-maintenance disponibilité des machines tournantes : modèles-mesurages-analyse des vibrations*, Masson, Paris (1995).

[17] E.G. Williams, J.D. Maynard, and E.Skudrzyk, *Sound source reconstructions using a microphone array*, Journal of the Acoustical Society of America, Vol. 68, No 1, (1980), pp. 340-344.

[18] E. G. Williams, *Fourier Acoustics*, Academic Press, New York (1999).

[19] E. G. Williams, *Regularization methods for near-field acoustical holography* Journal of the Acoustical Society of America, Vol. 110, No 4, (2001), pp. 1976-1988.